9-2011

A global comparison between station air temperatures and MODIS land surface temperatures reveals the cooling role of forests

David J. Mildrexler

Maosheng Zhao

Steven W. Running
University of Montana - Missoula

Recommended Citation

Mildrexler, D. J., M. Zhao, and S. W. Running (2011), A global comparison between station air temperatures and MODIS land surface temperatures reveals the cooling role of forests, J. Geophys. Res., 116, G03025, doi:10.1029/2010JG001486

JOURNAL OF GEOPHYSICAL RESEARCH, VOL. 116, G03025, doi:10.1029/2010JG001486, 2011

A global comparison between station air temperatures and MODIS land surface temperatures reveals the cooling role of forests

David J. Mildrexler,[1] Maosheng Zhao,[1] and Steven W. Running[1]

Received 21 July 2010; revised 13 May 2011; accepted 1 June 2011; published 30 August 2011.

[1] Most global temperature analyses are based on station air temperatures. This study presents a global analysis of the relationship between remotely sensed annual maximum *LST* (LST_{max}) from the Aqua/Moderate Resolution Imaging Spectroradiometer (MODIS) sensor and the corresponding site-based maximum air temperature (T_{amax}) for every World Meteorological Organization station on Earth. The relationship is analyzed for different land cover types. We observed a strong positive correlation between LST_{max} and T_{amax}. As temperature increases, LST_{max} increases faster than T_{amax} and captures additional information on the concentration of thermal energy at the Earth's surface, and biophysical controls on surface temperature, such as surface roughness and transpirational cooling. For hot conditions and in nonforested cover types, *LST* is more closely coupled to the radiative and thermodynamic characteristics of the Earth than the air temperature (T_{air}). Barren areas, shrublands, grasslands, savannas, and croplands have LST_{max} values between 10°C and 20°C hotter than the corresponding T_{amax} at higher temperatures. Forest cover types are the exception with a near 1:1 relationship between LST_{max} and T_{amax} across the temperature range and 38°C as the approximate upper limit of LST_{max} with the exception of subtropical deciduous forest types where LST_{max} occurs after canopy senescence. The study shows a complex interaction between land cover and surface energy balances. This global, semiautomated annual analysis could provide a new, unique, monitoring metric for integrating land cover change and energy balance changes.

Citation: Mildrexler, D. J., M. Zhao, and S. W. Running (2011), A global comparison between station air temperatures and MODIS land surface temperatures reveals the cooling role of forests, *J. Geophys. Res.*, *116*, G03025, doi:10.1029/2010JG001486.

1. Introduction

[2] Land surface temperature has been identified as one of the most important Earth System Data Records by NASA and other international organizations [*King*, 1999] and is a key variable in a wide variety of climate, hydrologic, ecological, biophysical, and biogeochemical studies [*Hansen et al.*, 2006; *Schmugge and Becker*, 1991; *Friedl and Davis*, 1994; *Mildrexler et al.*, 2009; *Nemani et al.*, 1996; *Running et al.*, 2004]. Surface temperatures are determined by land surface-atmosphere interactions and the energy fluxes between the atmosphere and the ground [*Mannstein*, 1987; *Sellers et al.*, 1988; *Jacob et al.*, 2004; *Jin and Dickinson*, 2010]. The surface energy balance components latent heat (*LE*) and sensible heat (*SH*) are strong functions of surface temperature [*Monteith*, 1981] and the apportionment of energy between them is governed by the dryness of the ground [*Priestley and Taylor*, 1972]. Full consideration of the surface energy balance shows that surface temperature is itself strongly governed by net radiation (*R*) and ground dryness [*Priestley and Taylor*, 1972]. Therefore surface temperature is a good indicator of the energy balance at the Earth's surface and is one of the key parameters in the physics of land surface processes on a regional as well as global scale [*Wan et al.*, 2004a].

[3] Climatological data can be developed for two kinds of surface temperatures: near-surface air temperature (T_{air}) and the skin temperature, or land surface temperature (*LST*) [*Jin and Dickinson*, 2010]. T_{air} is measured 1.5 m above the ground level at official weather stations with sensors protected from radiation and adequately ventilated [*Karl et al.*, 2006]. This common standard ensures the intercomparability between the measurements. The global average T_{air} trend is one of the key climate metrics used to assess the influence of anthropogenic activities on the climate system [*Hansen et al.*, 2006; *Pielke et al.*, 2007; *Intergovernmental Panel on Climate Change*, 2007]. Although correlated with T_{air}, *LST* differs from T_{air} in its physical meaning, magnitude, and measurement techniques [*Jin and Dickinson*, 2010]. *LST* can be estimated from measurements of thermal radiance coming from the land surface, retrieved from satellite, and mapped globally (section 1.1). The *LST* in the Moderate Resolution Imaging Spectroradiometer (MODIS) *LST* product is the radiometric (kinetic) temperature derived from the thermal infrared (TIR) radiation emitted by the land surface, and measured instantaneously [*Wan and Li*, 2011].

[1]Numerical Terradynamic Simulation Group, Department of Ecosystem and Conservation Sciences, University of Montana, Missoula, Montana, USA.

0148-0227/11/2010JG001486

Satellite-derived *LST* measures the canopy temperature in vegetated areas, a unique and useful ecological parameter because critical temperature-dependent physiological processes and associated energy fluxes occur in the vegetated canopy. The high-quality satellite-derived *LST* data sets, such as from MODIS, are currently used for a variety of applications including large-scale ecosystem disturbance detection [*Mildrexler et al.*, 2009; *Coops et al.*, 2009], drought monitoring [*Wan et al.*, 2004b], land cover monitoring [*Julien and Sobrino*, 2009], agrometeorology studies [*Anderson et al.*, 2007], biodiversity studies [*Albright et al.*, 2011], and have been proposed as an integrative global change metric [*Mildrexler et al.*, 2011]. In the remainder of this article, we use T_{air} to refer to the official weather station measurements taken 1.5 m above the land surface, and *LST* to refer to satellite-based skin temperature.

[4] The October 2008 *International Workshop on the Retrieval and Use of Land Surface Temperature* identified top issues for the Land Surface Temperature community research agenda (http://rain.atmos.colostate.edu/GRP/reports/NCDC-LSTWorkshopReport_final.pdf). Among the issues identified were to (1) demonstrate the usefulness of *LST* versus T_{air} for operational systems, (2) identify what additional information is provided by *LST* compared to T_{air}, and (3) evaluate the relationship between T_{air} and *LST* for different land surface types in terms of their diurnal cycle, diurnal range, monthly and annual averages, etc. In an analysis of the observed surface temperature data sets since 1950, *Pielke et al.* [2007, pp. 24–25] conclude, "If temperature trends are to be retained in order to estimate large-scale climate system heat changes (including a global average), the maximum temperature is a more appropriate metric than using the mean daily average temperature." This study provides additional understanding of the relationship between remotely sensed *LST* and site-based T_{air} in context of climate change and land cover change based on a global evaluation of the relationship between the annual maximum *LST* ($LST_{\max}$) and the corresponding maximum T_{air} ($T_{a\max}$). We compare the $LST_{\max}$ from the Aqua/MODIS sensor to the corresponding site-based $T_{a\max}$ for every World Meteorological Organization (WMO) station on Earth where $T_{a\max}$ is available, and analyze the relationship for different land cover types, and by WMO station location (e.g., latitude). Finally we analyze the spatial association between forest cover and $LST_{\max}$. Remote sensing offers the continuous spatial coverage needed to systematically compare $LST_{\max}$ and ground-based $T_{a\max}$ measurements from the global network of WMO stations. We are aware of one previous global study that has compared satellite-based *LST* to ground-based T_{air} measurements and evaluated the relationship by land cover type [*Jin and Dickinson*, 2010]. This global study is unique in its focus on the annual maximum *LST* and corresponding $T_{a\max}$.

1.1. Satellite-Derived LST and Surface Emissivity

[5] TIR remote sensing provides the possibility to retrieve surface temperatures and surface broadband emissivity in a spatially distributed manner and is therefore useful for estimating the temperature of heterogeneous surfaces such as soils and vegetation canopies [*Jacob et al.*, 2004; *Norman and Becker*, 1995]. The theoretical basis for remote sensing of *LST* is that the total radiance emitted by the ground increases rapidly with temperature [*Qin et al.*, 2001]. An infrared radiometer measures the thermal radiance that is coming from a surface within its instantaneous field-of-view (IFOV) and in some finite wavelength band [*Norman and Becker*, 1995]. Though atmospheric ozone absorbs most of the radiance from the ground in the 9.4–9.9 μm window, there is minimal loss for the radiance to transfer in the 10–13 μm range [*Qin et al.*, 2001]. The 10–13 μm range has been selected as the thermal channels for NOAA-AVHRR, Landsat thematic mapper, and the MODIS sensors aboard the Terra and Aqua platforms.

[6] The definition of *LST* in satellite remote sensing is based on Planck's law. Planck's law $B_\lambda(T)$ gives the dependence of spectral radiance L at a certain spectral band with wavelength λ emitted from a blackbody (i.e., surface emissivity $\varepsilon(\lambda) = 1$) on the body's kinetic temperature:

$$L_\uparrow = \varepsilon(\lambda)B(\lambda, T) \tag{1}$$

where $L_\uparrow$ is the radiance measured by the radiometer. The brightness temperature T^b can be found by inverting the Planck function for the blackbody's temperature using the observed spectral radiance ($T^b = B_\lambda^{-1}(L_\uparrow)$), where B^{-1} is the inverse of Planck's law. However, the emissivity of real objects is usually less than that of a perfect blackbody emitter. Also, heterogeneous surfaces like a plant canopy have nonuniform distributions of temperature and therefore are not simply related to a blackbody distribution at the same effective temperature [*Norman and Becker*, 1995]. Atmospheric gases, particularly water vapor, and clouds and aerosols also attenuate the surface radiance and add their own radiance impacting received radiance at the remote sensor level. Considering these effects, the general radiative transfer equation for remote sensing of *LST* [*Qin et al.*, 2001] can be stated as:

$$B_i(T_i) = \tau_i(\theta)\left[\varepsilon_i B_i(T_s) + (1 - \varepsilon_i)I_i^\downarrow\right] + I_i^\uparrow \tag{2}$$

where T_s is the *LST*, T_i is the brightness temperature in channel i, $\tau_i(\theta)$ is the atmospheric transmittance in channel i at viewing direction θ (zenith angle from nadir), and ε_i is the ground emissivity. $B_i(T_i)$ is the above-atmosphere radiance received by the sensor, $B_i(T_s)$ is the ground radiance, and $I_i^\downarrow$ and $I_i^\uparrow$ are the downwelling and upwelling atmospheric radiances, respectively [*Qin et al.*, 2001].

[7] While accurate estimation of surface emissivity and radiometric temperature from TIR remote sensing remains a difficult task due to atmospheric effects on spectral radiation transmission, variable emissivity, thermal characteristics of the ground, and different viewing angles of the sensor, substantial improvements have been made to the retrieval techniques over the past two decades [*Price*, 1984; *Wan and Li*, 1997]. Several temperature/emissivity separation algorithms have been developed. The MODIS *LST* suite comprises two algorithms; the generalized split window algorithm [*Wan and Dozier*, 1996], whose formula is similar to the split-window method used for AVHRR data [*Becker and Li*, 1990], and the physics-based day/night algorithm [*Wan and Li*, 1997]. The split-window *LST* method corrects the atmospheric effects based on the differential absorption in adjacent infrared bands and is used in the MODIS *LST* to retrieve *LST*s of clear-sky pixels by applying classification-

based emissivities in the split-window bands [*Snyder et al.*, 1998]. The day/night algorithm retrieves surface spectral emissivity and temperatures at 5 or 6 km grids from a pair of daytime and nighttime MODIS data in seven TIR bands [*Wan and Li*, 2011]. For more details on temperature/emissivity separation algorithms see [*Wan and Dozier*, 1989, 1996; *Wan and Li*, 1997; *Jacob et al.*, 2004].

1.2. The Influence of Vegetation on Surface Temperature

[8] The vegetated fraction of the Earth's surface influences climate through physical, chemical, and biological processes [*Bonan*, 2008; *Nemani et al.*, 1996]. Because plants are the primary site for the exchange of water, energy, and momentum between the land and atmosphere, vegetation has an important role in the climate system [*Hoffmann and Jackson*, 2000]. Plants leaves actively exchange absorbed solar radiation through evaporation and thereby maintain daytime canopy temperature close to the air temperature [*Gates*, 1965; *Nemani et al.*, 1993; *Waring*, 2002]. An increase in green biomass is often associated with a reduction in surface resistance to evapotranspiration, greater transpiration, a larger latent heat flux, and decreasing Bowen ratios [*Goward et al.*, 1985; *Nemani and Running*, 1989; *Lambin and Ehrlich*, 1996; *Mu et al.*, 2007]. Other qualities of vegetation, such as albedo and surface roughness also have very important impacts on surface-atmosphere energetics [*Bala et al.*, 2007; *Betts*, 2000; *Marland et al.*, 2003]. Alterations of the land surface cover type initiate a series of interactions and feedbacks in the climate-biosphere system [*Chapin et al.*, 2008]. Efforts to mitigate climate change with alterations to forestry and land management practices must factor in these biophysical changes and interactions [*Jackson et al.*, 2008; *Anderson et al.*, 2011].

[9] Each land cover type has distinct interactions with the atmosphere that can result in different local meteorological conditions. This reciprocal influence of vegetation on the microclimate of the particular area results from vegetation properties such as aerodynamic roughness, leaf seasonality, leaf area index, and partitioning of sensible and latent heat fluxes at the vegetation or ground surface [*Nemani et al.*, 1993]. The influence of vegetation on the expression of *LST* has been observed in disturbed and undisturbed areas across a range of spatial scales [*Lambin and Ehrlich*, 1996; *Nemani et al.*, 1996; *Mildrexler et al.*, 2006, 2009; *Running*, 2008].

[10] Until recently, the impacts of changes in land use on climate have generally been regarded as "noise" compared to the impacts of increases of greenhouse gases [*Kalnay et al.*, 2006]. However, recent studies suggest that the impact of widespread land use changes could be larger and should not be ignored [*Davey et al.*, 2006; *Hale et al.*, 2006; *Pielke et al.*, 2007; *Montenegro et al.*, 2009; *Loarie et al.*, 2011]. Quantification of the vegetation's influence on the thermal maxima of the land surface is important for understanding the role of different biomes in regulating the Earth's surface temperature, and the potential long-term impacts of land cover conversion on the surface energy balance.

[11] The degree to which different land cover types regulate the maximum surface temperature and how this varies between $LST_{\max}$ and $T_{a\max}$ is not well understood. The specific objectives of this study are to test the relationship between remotely sensed maximum *LST* and site-based maximum T_{air} and to examine the biophysical influence of each of the Earth's major land cover types on the expression of $LST_{\max}$ and $T_{a\max}$, to verify the hypotheses that $LST_{\max}$ will generally be higher than the corresponding site-based $T_{a\max}$ due to the greater concentration of thermal energy at the Earth's surface, and to investigate the effect of increased vegetation density on the relationship between $LST_{\max}$ and $T_{a\max}$. We are particularly interested in the biophysical interactions between terrestrial ecosystems and the atmosphere that cool regional weather extremes.

2. Data and Methods

2.1. Aqua/MODIS Instrument and LST Data

[12] Two MODIS instruments have been launched as part of the Earth Observing System (EOS). The first MODIS instrument on the Terra platform was launched on December 18, 1999 and the second MODIS instrument on the Aqua platform was launched on May 4, 2002. The strengths of the MODIS instruments are global coverage, high geolocation accuracy, high radiometric resolution, and accurate calibration in the visible, near-infrared and TIR bands [*Wan et al.*, 2004a]. The MODIS instruments have global coverage twice daily, resulting in nighttime and daytime data sets. The major advantages of the additional Aqua/MODIS data for the *LST* product include the increase in quantity and the improvement in quality of the emissivity and temperature science data over the global land due to the increasing number of MODIS observations in clear-sky conditions [*Wan et al.*, 2004a].

[13] The MYD11C2 Aqua/MODIS 8 day *LST* Climate Model Grid (CMG) data used to create global maps of annual maximum *LST* has a spatial resolution of 0.05° (approximately 5.6 km at the equator) and is aggregated from 1 km *LST* data. The primary source of the *LST* data in the series of MYD11C products is the physics-based day/night algorithm developed to retrieve surface spectral emissivity and temperature at 5 km resolution from a pair of daytime and nighttime MODIS data in seven TIR bands [*Wan and Li*, 1997]. The *LST* algorithm is capable of adjusting to uncertainties in atmospheric temperature and water vapor profiles for a better retrieval of the surface emissivity and temperature without a complete simultaneous retrieval of surface variables and atmospheric profiles [*Wan et al.*, 2004a]. In most cases MODIS *LST* data are accurate within 1K [*Wan et al.*, 2003, 2004a].

[14] *LST* from the Aqua/MODIS sensor was chosen for this study because of Aqua's afternoon overpass time of approximately 13:30 local time. Compared to the Terra/MODIS sensor's overpass time of 10:30 local time, Aqua's afternoon overpass retrieves *LSTs* that are much closer to the maximum daily temperature of the land surface. Measurements close to the peak of diurnal fluctuation better reflect the thermal response of rising leaf temperatures due to decreased latent heat flux as stomata close, and soil litter surfaces dry, accentuating differences in *LST* among vegetation covers [*Mildrexler et al.*, 2007]. As a result, it is more suitable for some regional and global change studies [*Wan et al.*, 2004a] and is particularly well-suited for those utilizing a maximum *LST* compositing approach. The MODIS *LST* bands based on TIR data are only available under clear

sky conditions because clouds inhibit satellite observations in the visible and TIR spectral ranges. Because $LST_{\max}$ occurs in clear sky conditions, selection of annual maximum *LST* can simultaneously solve the cloud contamination issue, an inherent problem for optical remote sensing, especially over woody ecosystems [*Zhao et al.*, 2005].

2.2. MODIS Land Cover Data

[15] The MOD12Q1 Terra/MODIS collection 4 Land Cover data set has a spatial resolution of 1 km. The primary objective of the MODIS land cover product is to facilitate the inference of biophysical information for use in regional and global modeling studies and therefore must be discernible with high accuracy and directly related to physical characteristics of the surface, especially vegetation [*Friedl et al.*, 2002]. A classification scheme that groups the Earth's surface into 17 major classes was developed by the International Geosphere-Biosphere Programme (IGBP) specifically for this purpose and is used in the MODIS land cover product [*Loveland and Belward*, 1997; *Friedl et al.*, 2002]. The MODIS land cover provides a consistent grouping method and the means to explore the land cover specific relationship between $LST_{\max}$ and $T_{a\max}$ within a biogeographic context. The weakness of this approach is that the MODIS land cover is an aggregate classification for the entire pixel, whereas the localized land use patterns directly around the weather station can have large impacts on the local meteorological conditions [*Davey et al.*, 2006; *Hale et al.*, 2006]. To overcome this we analyze the entire global data set and assess the general trends in the $LST_{\max}$ and $T_{a\max}$ relationship. The MODIS land cover data is also useful for examining the spatial association between land cover type and the $LST_{\max}$ across the land surface. To match the spatial resolution of the Aqua/MODIS *LST* CMG data set, the MODIS 1 km land cover data set was aggregated to 0.05° and the dominant land cover was chosen from the 6×6 km window.

2.3. World Meteorological Organization Data

[16] Global daily WMO weather station data from over 10,000 weather stations located around the world can be obtained at the NOAA NCDC webpage at ftp://ftp.ncdc.noaa.gov/pub/data/gsod/ish-history.txt. The daily maximum air temperature is one of the daily variables available in this data set. However, not all of the different stations include each of the variables all of the time.

2.4. Data Processing

[17] We obtained the MYD11C2 MODIS *LST* (CMG) data from 2002 to 2006, and 2009. Annual maximum value compositing was applied to the *LST* data, selecting independently for each pixel the maximum 8 day *LST* over a 1 year period from all 8 day composites labeled as reliable by the quality control (QC). A key advantage of annual maximum composite *LST* data is that it removes the influence of synoptic weather variability that influences satellite based *LST* at daily, weekly and seasonal timeframes [*Lambin and Ehrlich*, 1996; *Nemani and Running*, 1997]. With this approach the upper limit of surface temperature can be examined synchronously over the Earth's surface.

[18] At each WMO site we extracted the station location (i.e., latitude and longitude), the corresponding MODIS pixels $LST_{\max}$, and the corresponding $T_{a\max}$ on the date of the 8 day $LST_{\max}$ from 2002 to 2006. To temporally match the annual maximum 8 day composite MODIS *LST* data, correspondingly, we averaged the daily maximum air temperature into 8 day periods. We also extracted the MODIS land cover for every pixel so that the data set could be stratified and the $LST_{\max}/T_{a\max}$ relationship analyzed by land cover type. The 2009 $LST_{\max}$ is used in the final comparison with the MODIS land cover.

3. Results and Discussion

[19] Figure 1 illustrates the global network of WMO weather stations and the MODIS IGBP Land Cover classification used in this analysis. The distribution of weather stations is heavily biased toward the Northern Hemisphere, especially the United States and Europe, resulting in some land cover types having much greater representation than others. Note the paucity of stations in the tropical forests, savannas, shrublands and barren areas.

[20] First, we examine the overall relationship between $LST_{\max}$ from the Aqua/MODIS sensor and the corresponding site-based $T_{a\max}$ with all land covers combined. Second, we analyze the land cover specific relationship between $LST_{\max}$ and $T_{a\max}$. Finally, we provide biogeographic examples of large-scale regulation of the surface temperature focusing on forests.

3.1. LST_{max}-T_{amax} Comparison

[21] The global comparison between the Aqua/MODIS $LST_{\max}$ and the corresponding WMO site-based $T_{a\max}$ for the same 8 day time period is shown in Figure 2 for 2003–2006. A dashed line is included in the scatterplots to illustrate divergence from a 1:1 relationship.

[22] $LST_{\max}$ tends to be hotter than $T_{a\max}$ and the difference increases with increasing temperature (Figures 2a–2d). For all 4 years $T_{a\max}$ stays below 50°C whereas $LST_{\max}$ exceeds 60°C. The $LST_{\max}$ can be 20°C hotter than the corresponding $T_{a\max}$ at these upper temperatures. The difference is potentially even greater considering that the MODIS *LST* is an aggregation of the radiometric signal from the entire 5×5 km^2 pixel footprint. The large difference between $LST_{\max}$ and $T_{a\max}$ at these high temperatures captures the important distinction between a radiative measurement taken at the surface of the earth where thermal energy is most concentrated and an air temperature measured 1.5 m above the ground. As temperature decreases, the progressive coupling of the $LST_{\max}/T_{a\max}$ relationship can be generally attributed to an increase in vegetation density. This is mainly due to transpirational cooling lowering the Bowen ratios, and to the greater aerodynamic roughness of the vegetated areas enhancing cooling through turbulent exchange. The land cover specific analysis that follows allows for more in-depth investigation into the biophysical influences on the $LST_{\max}/T_{a\max}$ relationship.

[23] To examine the latitudinal variation in the $LST_{\max}/T_{a\max}$ relationship, the 4 years of data were combined into one data set and then the differences between $LST_{\max}$ and $T_{a\max}$ were calculated for each site. Next, the site specific differences were plotted against the corresponding latitude for each WMO station, with positive and negative values indicating the Northern and Southern hemispheres, respec-

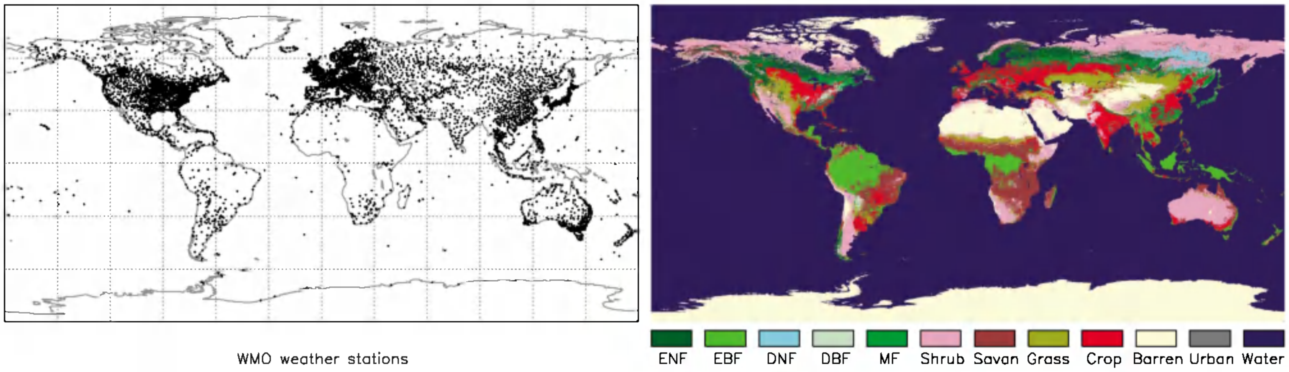

Figure 1. (left) Location of WMO weather stations where $T_{a\max}$ and the corresponding MODIS pixels $LST_{\max}$ and land cover type were extracted. (right) MOD12Q1 land cover data set with classification system defined as Evergreen Needleleaf Forest (ENF), Evergreen Broadleaf Forest (EBF), Deciduous Needleleaf Forest (DNF), Deciduous Broadleaf Forest (DBF), Mixed Forests (MF), Closed Shrublands (CShrub), Open Shrublands (OShrub), Woody Savannas (WSavan), Savannas (Savan), Grassland (Grass), Croplands (Crop), and Barren. Note that here we combined CShrub and OShrub into Shrub, and Woody Savannas and Savannas into Savan.

tively (Figure 3). We do not imply the use of latitude as a surrogate for solar radiation. Latitude is useful for this analysis because it provides a biogeographical context for contrasting the $LST_{\max}/T_{a\max}$ relationship. The scatterplot shows that across all latitudes the $LST_{\max}$ is usually hotter than the $T_{a\max}$, but there are some very large differences. While the inequitable distribution of WMO stations across the global surface has a strong influence on the distribution of data points, especially the greater number of stations in the Northern Hemisphere, there appears to be a general bimodal distribution (Figure 3). At the equator, $LST_{\max}$ and $T_{a\max}$ tend to be more coupled. Moving away from the equator, an increasing number of sites begin to have much higher $LST_{\max}$ with the difference peaking at about 25°C between ±25° to ±40° latitude. The relationship progressively couples again moving toward the poles, where the

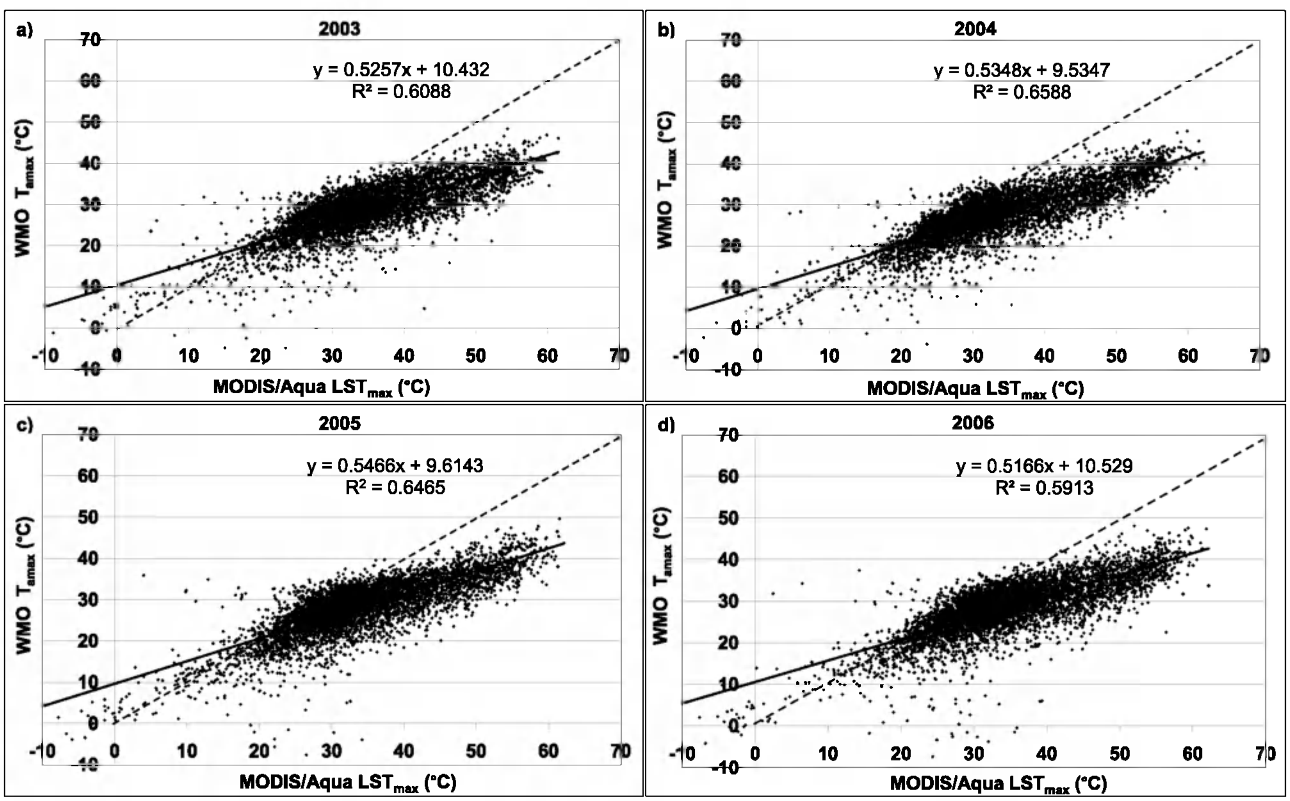

Figure 2. Observed relation between station-based $T_{a\max}$ and satellite-derived $LST_{\max}$ for 2003–2006. Each point represents one WMO station and the corresponding MODIS pixel, and the dashed line shows the 1:1 relationship.

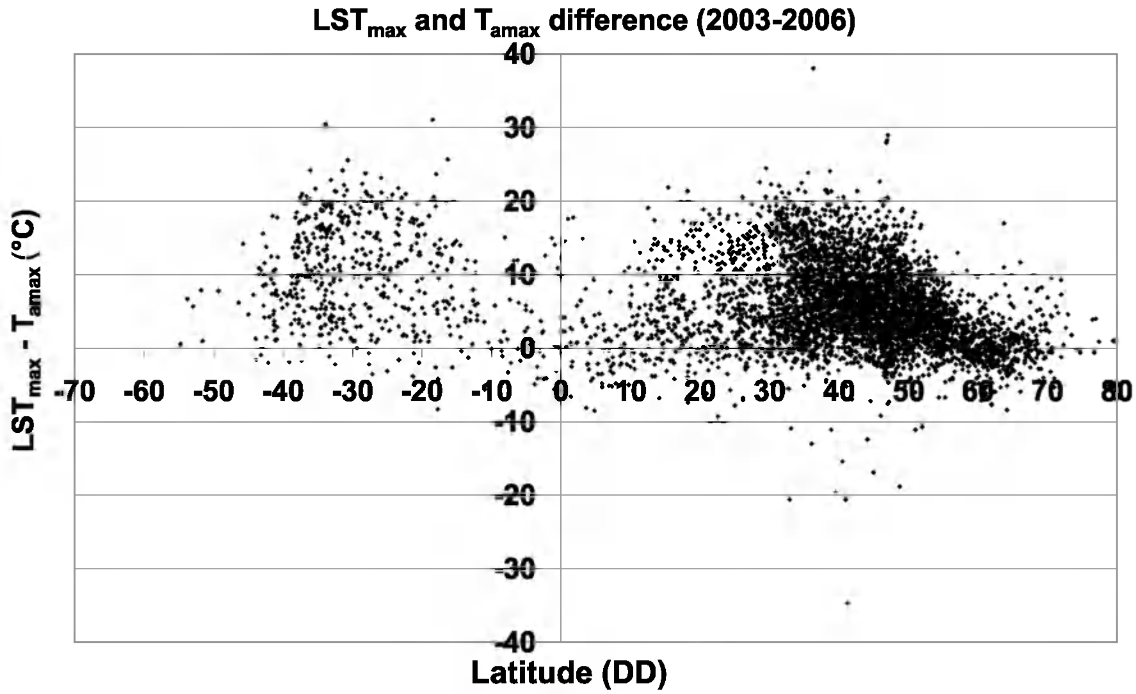

Figure 3. LST_{max} is generally higher than the corresponding T_{amax} across all latitudes with maximum amplitude occurring at the midlatitudes.

Northern Hemisphere weather stations are located in year-round cold environments. Sites where the T_{amax} is hotter than the LST_{max} are indicated by the negative values and mostly range between 0°C and 10°C higher than the corresponding LST_{max}.

3.2. Land Cover Specific Comparison

[24] When the Earth's major land cover types are analyzed within the surface temperature-vegetation index space, a trajectory results where increasing vegetation density is coupled with decreasing *LST* [*Nemani and Running*, 1989; *Lambin and Ehrlich*, 1996; *Mildrexler et al.*, 2007]. The negative relation between remotely sensed vegetation indices (*VIs*) (e.g., Normalized Difference Vegetation Index (*NDVI*), Enhanced Vegetation Index (*EVI*)) and *LST*, indicates changing energy absorption and exchange characteristics, and the gradient in Bowen ratios of various land cover types. Our analysis of the biophysical influence of different land cover types on the expression of LST_{max} and T_{amax} follows the *LST-VI* relationship, beginning with barren landscapes (high *LST*, low *EVI*) and ending with forests (low *LST*, high *EVI*).

3.2.1. Barren Areas

[25] Barren lands are characterized by exposed soil, sand, rocks or snow and cover 24.1% of the global land area. Hot and cold deserts contain large numbers of pixels classified as barren (see Figure 1), and this biogeographic distribution is reflected by the grouping of data points at the extreme high and low ends of the temperature spectrum (Figure 4a). The scatterplot for barren areas indicates how much LST_{max} differs from T_{amax} in areas that are mostly devoid of vegetation. The WMO stations in polar regions (60°N–80°N)

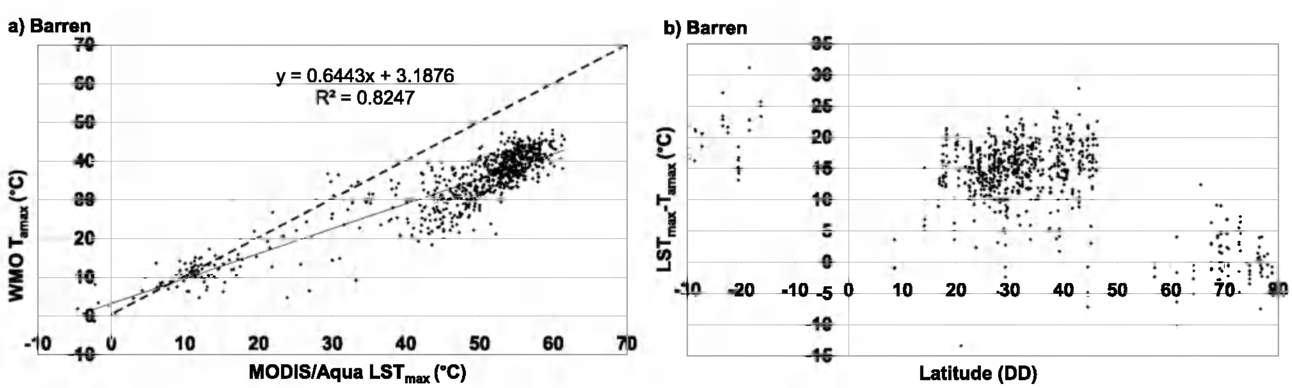

Figure 4. Observed LST_{max}/T_{amax} relationship for barren areas (a) reflects biogeographic distribution in extreme temperature environments and (b) illustrates how much more the LST_{max} increases in response to increased incoming solar radiation than the corresponding T_{amax}.

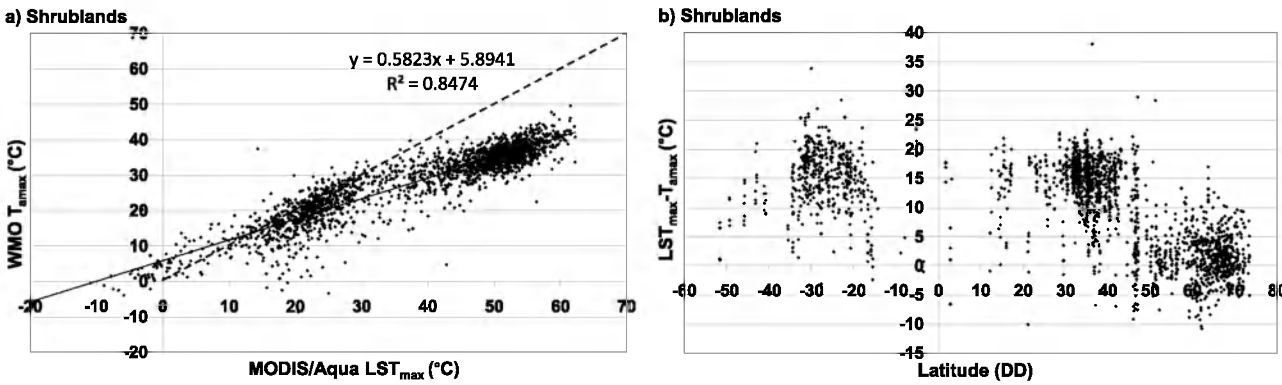

Figure 5. (a) Observed $LST_{max}/T_{a\max}$ relationship for shrublands is similar to barren areas with a temperature distribution in both extreme hot and cold environments. (b) While LST_{max} and $T_{a\max}$ approximate the 1:1 relationship in high-latitude year-round cold environments, in hot deserts LST_{max} is more closely coupled to the radiative and thermodynamic characteristics of the Earth's surface than $T_{a\max}$.

have the lowest temperatures, and the $LST_{max}/T_{a\max}$ relationship approximates a 1:1 relationship (Figure 4b). In these year-round cold environments, the exposed ground is covered in snow or ice, or stays moist through the short summers. Snow and ice-covered areas reflect the incoming solar radiation thereby maintaining low LST_{max}, and moist soil conditions greatly restricts the increase in surface temperature as absorbed solar radiation is consumed in evaporation [*Nemani and Running*, 1989; *Nemani et al.*, 1993; *Friedl and Davis*, 1994]. As temperature goes up, and more thermal energy is concentrated at the Earth's surface, LST_{max} increases much more rapidly than $T_{a\max}$, and at the highest temperatures, LST_{max} exceeds 60°C, whereas $T_{a\max}$ stays below 50°C (Figure 4a). Significantly higher LST_{max} temperatures have been remotely sensed, but the Earth's hot deserts such as the Sahara, the Gobi, the Sonoran, and the Lut, are climatically harsh and so remote that access for routine measurements and maintenance of a weather station in these areas is impractical [*Mildrexler et al.*, 2011].

[26] These results are supported by physical considerations which indicate that the most extreme maximum temperatures will occur at bare-soil surfaces under full solar illumination and low wind speed, where the soil is dry and has a very low albedo and low thermal conductivity [*Garratt*, 1992]. Field studies also corroborate these results. In an analysis of the temperature conditions of air and soil conducted in the desert near Tucson, Arizona, a maximum soil temperature of 71.5°C (160.7°F) was measured 0.4 cm below the soil surface at 1:00PM on June 21, 1915 [*Sinclair*, 1922]. The corresponding air temperature measured 4 ft above the ground was 42.5°C (108.5°F) [*Sinclair*, 1922]. Other studies that have observed extreme maximum surface temperatures and air temperatures near the time of the observed surface temperature have found differences of even greater magnitude [*Peel*, 1974].

3.2.2. Shrublands

[27] This MODIS land cover class covers 19.2% of the global land area and includes open and closed shrublands. Open shrublands are characterized by woody vegetation less than 2 m tall and with shrub canopy cover ranging between 10 and 60%. Closed shrublands are characterized by lands with woody vegetation less than 2 m tall and greater than 60% shrub canopy cover. Closed shrublands occupy only a tiny fraction of the Earth's surface compared to open shrublands and for this analysis closed and open shrublands are combined together. The $LST_{max}/T_{a\max}$ relationship for shrublands displays a pattern similar to barren areas where the data points are clustered in extreme hot and cold environments (Figure 5a). The shrublands land cover class includes the Northern Hemisphere WMO stations located within the tundra biome where the $LST_{max}/T_{a\max}$ relationship is near 1:1 (Figure 5b). The tundra biome is characterized by cold, desert-like conditions, short growing seasons, permafrost, and a plant community composed of grasses such as tussocks and low-lying shrubs. With adequate water for evapotranspiration, this energy limited system always has low Bowen ratios and low surface temperatures [*Nemani and Running*, 1997]. As temperature increases, LST_{max} increases much more rapidly than the corresponding $T_{a\max}$, until at the highest temperatures, LST_{max} is between 10°C and 25°C higher (Figure 5b). These data points represent hot, arid shrubland communities located within the ±15° to ±45° latitude range such as in the interior of Australia, the Kalahari Desert in southern Africa, the Patagonian Desert in Argentina, and the Great Basin in the interior western United States.

[28] Fractional vegetation cover has a key influence on the expression of maximum surface temperature in the shrubland biome. Leaves, even if not transpiring, are considerably more efficient at shedding absorbed energy than are soil surfaces, and have significantly cooler surface temperature than bare soil [*Choudhury*, 1989]. Therefore, surface temperature tends to vary directly with the proportion of soil within the sensor IFOV [*Friedl and Davis*, 1994]. This phenomenon has been well documented and is a key reason why hot, dry, open shrublands have such high LST_{max} compared with $T_{a\max}$. In the cold shrubland environments, fractional vegetation coverage does not result in high surface temperatures because the exposed ground is covered in snow or ice, or stays moist through the short summers, thereby greatly restricting the increase in surface temperature.

3.2.3. Grasslands

[29] Grasslands cover 8.6% of the global land area and are dominated by herbaceous types of cover and are characterized by semiarid climates with substantial precipitation

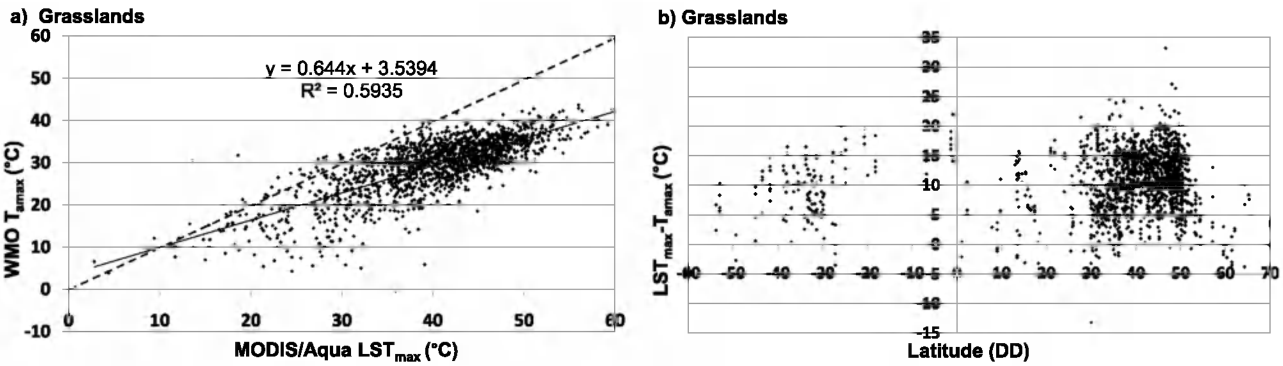

Figure 6. (a) Observed LST_{max}/T_{amax} relationship for grasslands and (b) their distribution in middle latitudes. Extreme maximum temperatures occur during the hottest and driest part of the year after grasses have senesced. Fractional vegetation cover and soil background elements within the sensor's IFOV contribute to the high LST_{max} values.

variability. These water-limited ecosystems, such as the grasslands of the central United States, display high interannual variability in annual net primary productivity (ANPP) in response to precipitation variability [*White et al.*, 2005; *Knapp and Smith*, 2001]. The LST_{max}/T_{amax} scatterplot illustrates the relatively warm, mild temperature envelope that grasslands occupy compared with barren and shrubland cover types (Figure 6a).

[30] Most of the WMO weather stations in grasslands are located in the Northern Hemisphere and in warm, middle latitudes (Figure 6b). Grasslands, with their shallow, fibrous root systems, are not able to sustain transpiration through the hot, dry periods when the most extreme annual maximum temperatures occur. Under conditions with low wind speed, turbulent heat transfer in grasslands is minimal due to their relatively low and homogenous canopy surface area. Fractional vegetation coverage including soil background elements is also important in grasslands and the effective surface temperature is proportional to the amount of soil versus canopy within the sensor IFOV [*Friedl and Davis*, 1994]. Combined these factors result in the potential for a large apportionment of incoming solar radiation to sensible heat with high LST_{max} values between 50°C and 60°C.

3.2.4. Croplands

[31] Croplands cover 11.9% of the global land area and are defined as land covered with temporary crops followed by harvest and a bare soil period and includes both irrigated and nonirrigated croplands. Just as rainfall enhances vegetation density and thereby lowers LST_{max}, irrigation can artificially enhance vegetation density in the same way. *Mildrexler et al.* [2006] showed that an intensively irrigated *Populus* tree farm had an LST_{max} of 33.0°C in 2003, and 36.0°C in 2005, over 25°C cooler than the nearby semiarid, natural, shrubland cover type. This agrees fairly well with previous research that has shown that surface temperatures of well watered closed canopies do not rise above 32°C to 34°C [*Linacre*, 1964; *Gay*, 1972; *Priestley and Taylor*, 1972]. The LST_{max}/T_{amax} relationship illustrates that whereas T_{amax} increases very gradually from 30°C to 40°C, LST_{max} increases much faster (Figure 7a). The progressive decoupling of the LST_{max}/T_{amax} relationship at higher temperatures is likely capturing a shift toward more arid landscapes that are not irrigated, or where irrigation is limited to the early growing season and crops are harvested before annual maximum temperatures occur. Once the ecosystem

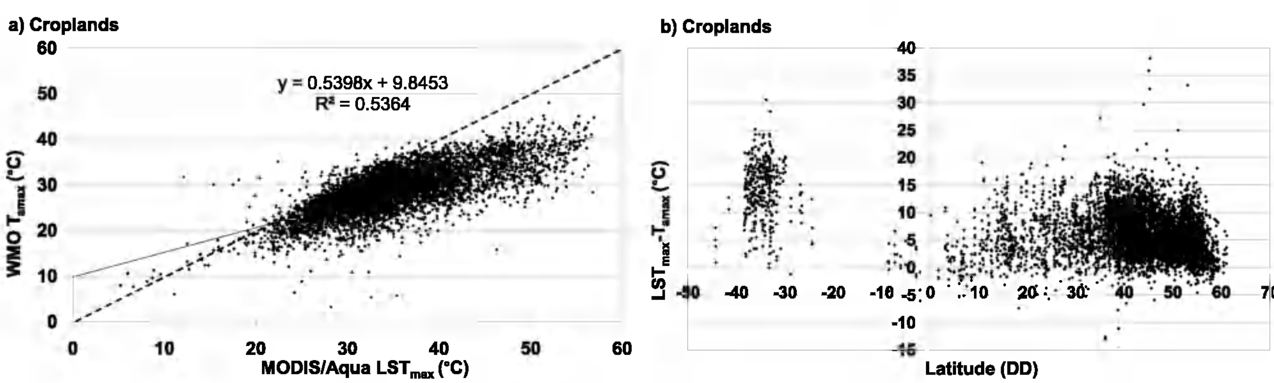

Figure 7. (a) Observed LST_{max}/T_{amax} relationship for croplands is well coupled from 20°C to 35°C, partly due to the artificial reduction of LST_{max} due to irrigation. Above 35°C, LST_{max} increases much more rapidly than T_{amax} indicating arid areas without irrigation or where irrigation is limited to the early growing season. (b) The greater difference between the LST_{max} and T_{amax} in the Southern Hemisphere reflects farming in very arid areas.

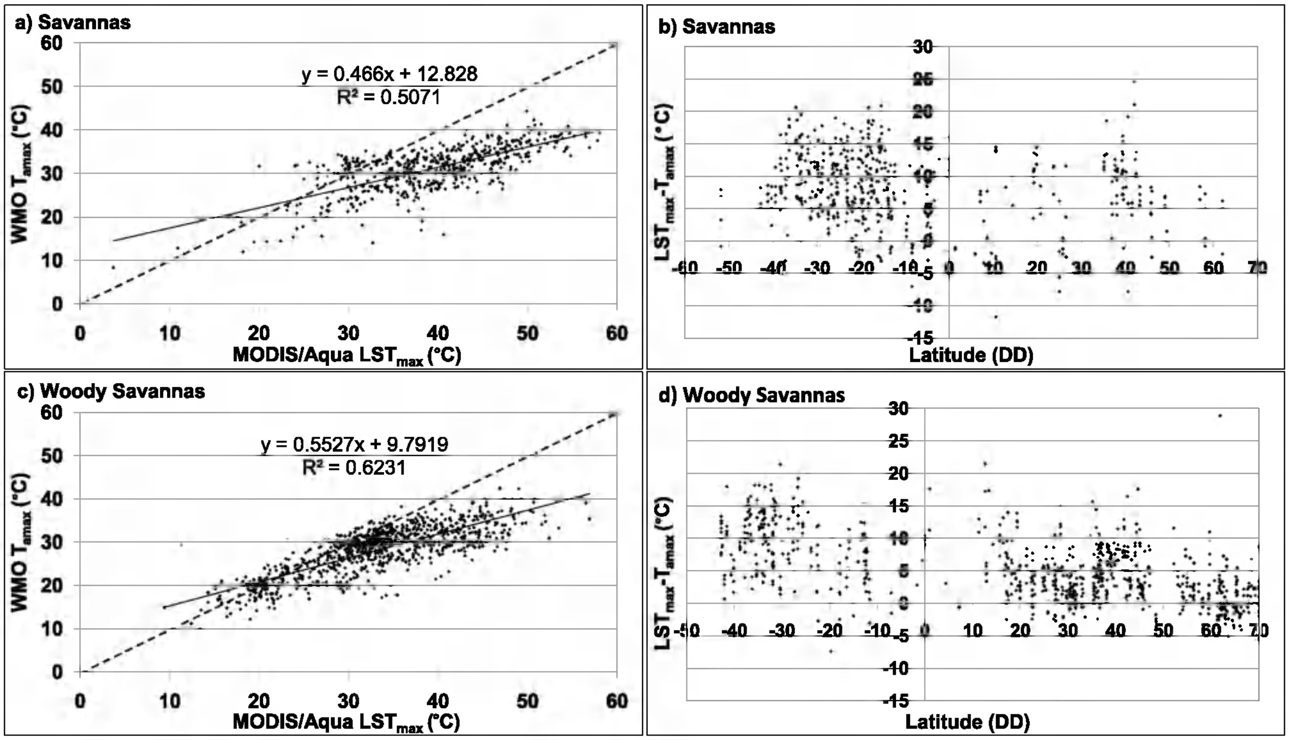

Figure 8. Observed $LST_{\max}/T_{a\max}$ relationship for (a, b) savannas and (c, d) woody savannas. Stomata are shut in savannas trees when extreme maximum temperatures occur, and the affect of increased surface roughness on the $LST_{\max}/T_{a\max}$ relationship in woody savannas can be observed. Woody savannas have a boreal and subarctic woodland component in the Northern Hemisphere where $LST_{\max}$ and $T_{a\max}$ are tightly coupled (Figure 8d).

dries down and harvest exposes bare ground, the $LST_{\max}$ exceeds 55°C and the $T_{a\max}$ reaches 45°C.

[32] Croplands extend across a very large latitudinal gradient in the Northern Hemisphere (Figure 7b). In the Southern Hemisphere the WMO stations in croplands are located in a very narrow latitudinal band and the average temperature difference between the $LST_{\max}$ and the $T_{a\max}$ tends to be larger than in the Northern Hemisphere. This reflects less irrigation and farming in more arid areas in the Southern Hemisphere as can be seen by the proximity of croplands to arid, shrubland environments in Australia, southern Africa, and South America (Figure 1). In the Northern Hemisphere, croplands border forests and grasslands.

3.2.5. Savannas

[33] Savannas and woody savannas cover 13.7% of the global land area and are defined as lands with forest canopy cover ranging between 10–30% and 30–60%, respectively, and with herbaceous and other understory systems. This MODIS land cover class is defined by tree cover and therefore includes boreal and subarctic woodlands in addition to the subtropical belt savannas of Brazil, Africa, and Australia. The presence of trees incorporates a greater structural complexity into the savanna environment. Woody savannas and savannas are analyzed separately because changes in woody vegetation cover has been shown to have a marked difference on the partitioning of available energy into sensible and latent heat exchanged in the savanna environment [*Hoffmann and Jackson*, 2000; *Baldocchi et al.*, 2004].

[34] The scatterplots illustrate that the $LST_{\max}/T_{a\max}$ relationship for savannas (Figure 8a) is shifted toward a higher temperature distribution compared to woody savannas (Figure 8c). The average $T_{a\max}$ is 31.1°C for savannas and 29.3°C for woody savannas. While the $T_{a\max}$ upper limit is very similar for savannas and woody savannas, the $LST_{\max}$ upper limit is higher for savannas. This results in a larger difference between $LST_{\max}$ and $T_{a\max}$ in savannas than in woody savannas in warm subtropical latitudes (Figures 8b and 8d). Tree cover can be as low as 10% in savannas and during the hot, dry conditions when annual maximum temperatures occur, the understory vegetation will have dried down, further exposing soil background elements. These factors contribute to the higher $LST_{\max}$ for savannas compared with woody savannas. Also, the more forested woody savannas have a higher surface roughness that increases the conduction of sensible and latent heat from the surface to the atmosphere, lowering surface temperature [*Hoffmann and Jackson*, 2000]. During the hot dry summer, stomata shut in the savannas trees, and sensible heat fluxes greatly increase [*Baldocchi et al.*, 2004].

[35] At the lowest temperatures the $LST_{\max}/T_{a\max}$ relationship for woody savannas is near 1:1 (Figure 8c). These are the WMO stations at high latitudes within the boreal and subarctic woodlands where water is not limiting, and low Bowen ratios and low surface temperature are maintained through the short growing season (Figure 8d).

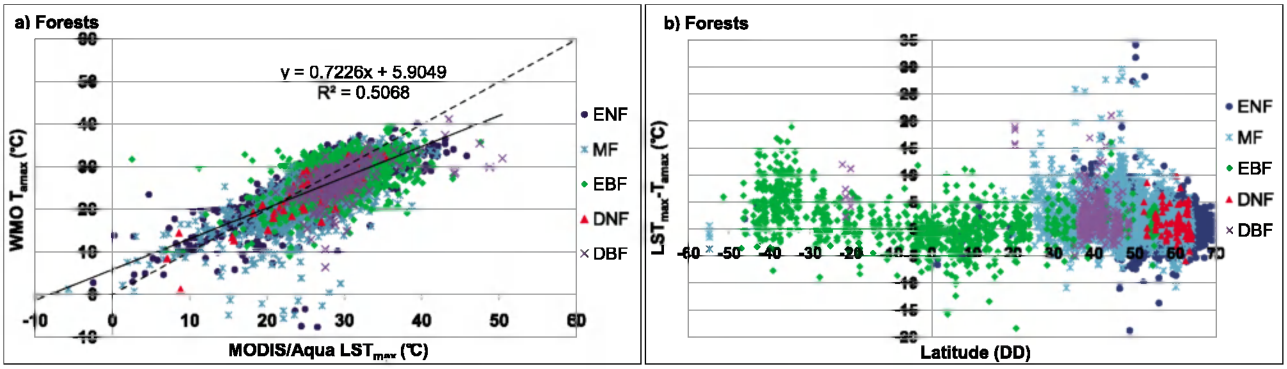

Figure 9. Observed LST_{max}/T_{amax} relationship for forests (ENF in dark blue, MF in light blue, EBF in green, DNF in red, and DBF in purple) illustrates that (a) LST_{max} and T_{amax} generally range between the same values, (b) across a very broad latitudinal range. Even during annual maximum temperatures, forests maintain canopy temperatures close to air temperature mainly through transpirational cooling and secondarily through high surface roughness that enhances turbulent exchange.

3.2.6. Forests

[36] Forests cover 21.9% of the global land area and include all sites classified as evergreen broadleaf forest (EBF), deciduous broadleaf forest (DBF), evergreen needleleaf forest (ENF), deciduous needleleaf forest (DNF), and mixed forest (MF). All of the forested cover types are characterized by at least 60% tree canopy cover, and are distinguished by color in the scatterplot. Across the temperature range the LST_{max}/T_{amax} relationship for forests approximates the 1:1 line much more closely than the other cover types (Figure 9a). For forests both the LST_{max} and the T_{amax} tend to range between the same values, approximately 15°C to 40°C. This illustrates the unique atmospheric coupling of forests where canopy temperatures are maintained closer to that of the surrounding air temperature. This is primarily attributed to the fact that even during the conditions when maximum temperatures occur, forests are able to access water with their deep root systems and continue transpiration. A greater proportion of incoming solar radiation is partitioned to latent heat flux as a result of rapidly transpiring vegetation, thereby cooling the canopy surface temperature. Additionally, forests have deep, complex canopies that promote cooling through turbulent exchange.

[37] Forests cover a broad latitudinal range making their relatively narrow range of maximum temperatures all the more remarkable (Figure 9b). The atmospheric coupling of forest ecosystems is illustrated by the grouping of the sites around the x axis indicating a small difference between LST_{max} and T_{amax}. Forests have more sites where the T_{amax} is warmer than the corresponding LST_{max} compared to the other cover types. *Priestley* [1966] examined the average daily maximum temperature for each month reported by island observing stations and by land stations and concluded that air temperatures over a well watered surface do not rise above 32°C to 34°C. The T_{amax} from the WMO sites in all forest types levels off about 35°C (Figure 9a). *Priestley* [1966] specifically focused on the average daily maximum temperature following periods of heavy rain, whereas the LST_{max}, and hence the corresponding T_{amax}, occurs under drier conditions.

3.3. Forests and Maximum LST Spatial Association

[38] Having analyzed the biophysical influence of specific land cover types on the LST_{max}/T_{amax} relationship, we now examine the association between the spatially continuous satellite-derived MODIS LST_{max} and land cover data sets. We focus on forests because they sustain the hydrologic cycle through evapotranspiration which contributes to a cooling of climate through feedbacks with clouds and precipitation [*Bonan*, 2008]. Based on the forests scatterplot we assign 38°C as the approximate upper limit of LST_{max} for forests (Figure 9a) and expect a close spatial correspondence between the location of forests and LST_{max} that does not exceed the upper limit. Savannas are examined because of their higher surface roughness that lowers surface temperature. An example of the influence of irrigation on LST_{max} in an arid landscape is also provided.

[39] The 2009 LST_{max} for Central Africa has a large contiguous area that does not exceed 38°C (Figure 10a; in blue). This area corresponds to the location of the Congo rain forest (Figure 10b; in green). Smaller patches of forest cover can be seen in the surrounding areas that show strong spatial association with LST_{max} values that do not exceed 38°C. This illustrates the important role of large contiguous blocks, and small isolated patches of forest at regulating LST_{max}. Most of the nonforest areas that have LST_{max} below 38°C correspond to the location of woody savannas (Figure 10b; in brown). Woody savannas tend to occupy the border of forests, and then transition into savannas, with their much lower forested cover. Savannas are associated with LST_{max} in the 40°C to 55°C range. This demonstrates the importance of forests and savannas in moderating surface temperatures across the African continent, and the different magnitude of the influence on the LST_{max} from tropical forests that sustain transpiration through the dry season, and savannas that do not sustain transpiration, but have high surface roughness.

[40] The entire tropical forest belt extending across the Amazon (Figures 11a and 11b), Southeast Asia, and Indonesia, shows a very close association between the location of forests and LST_{max} that does not exceed 38°C. The cooling role of tropical forests is pronounced as the

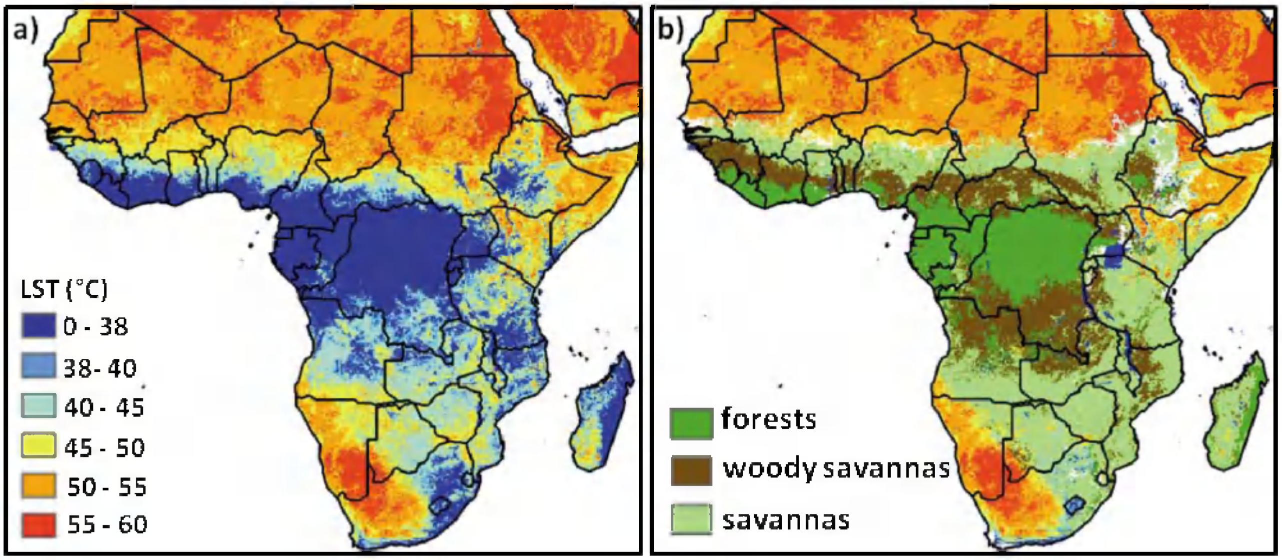

Figure 10. The (a) 2009 LST_{max} for Africa and (b) spatial correspondence between forests and temperatures that do not exceed 38°C. This demonstrates the different magnitude of the influence on LST_{max} from tropical forests that sustain transpiration through the dry season, and savannas that do not, but have high surface roughness.

hydrologic cycle is tightly coupled with forests [*Nemani et al.*, 1996; *Bonan*, 2008]. Observations from flux towers in the Brazilian Amazon support this and show that forest transpiration is sustained during the dry season [*Hutyra et al.*, 2007; *Bonan*, 2008]. Some areas in the Amazon where forest cover loss due to deforestation is confirmed, such as within the state of Mato Grosso [*Morton et al.*, 2006; *Hansen et al.*, 2008], show an increase in LST_{max} relative to surrounding forested areas (Figure 11b). Studies that examine the potential of forests for climate mitigation, which requires a holistic evaluation of biophysical factors, suggest that tropical forests provide the greatest climate value, because carbon storage and biophysics align to cool the Earth [*Jackson et al.*, 2008].

[41] The DBF areas south of the Amazon have high LST_{max} values compared to the nearby EBF areas (Figures 11a and 11b). The subtropical DBF biome has long dry seasons during which trees shed their leaves. The LST_{max} occurs after canopy senescence negating transpirational cooling. The LST_{max}/T_{amax} relationship for DBF forests presented in Figure 9 shows some very high temperatures, but too few sites to draw conclusions. This

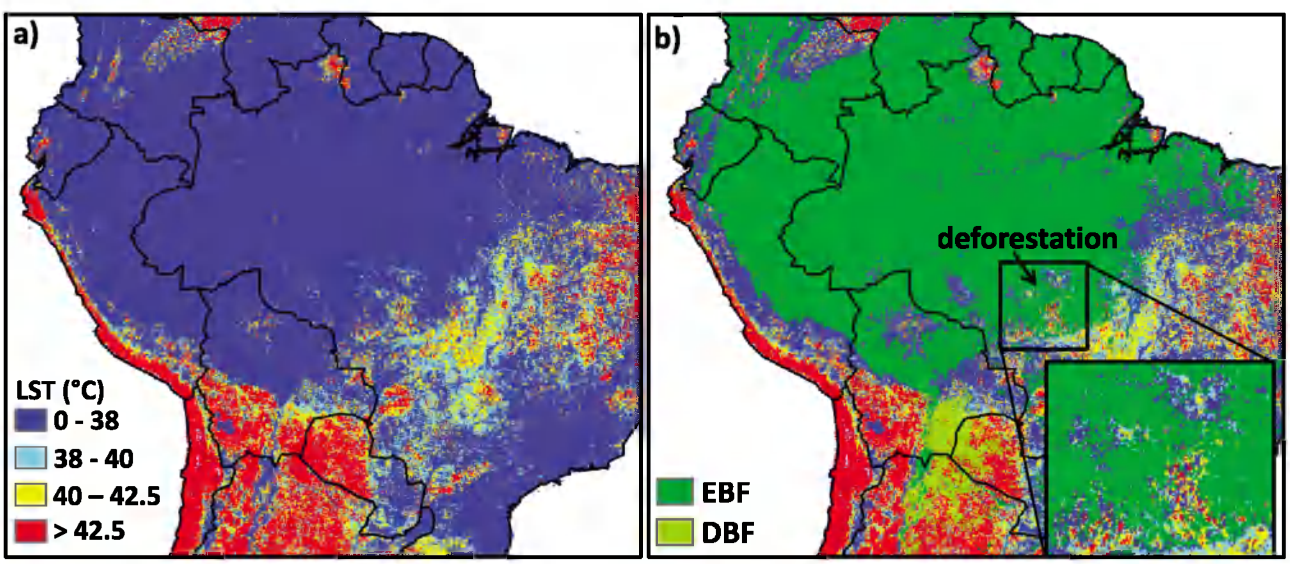

Figure 11. (a) The 2009 LST_{max} across the Amazon Basin and (b) the spatial correspondence between forests and temperatures that do not exceed 38°C. Note the LST_{max} scale is changed to draw out the affect of deforestation on LST_{max}. Tropical DBF forests have LST_{max} values above 45°C because maximum temperatures occur after trees have shed their leaves.

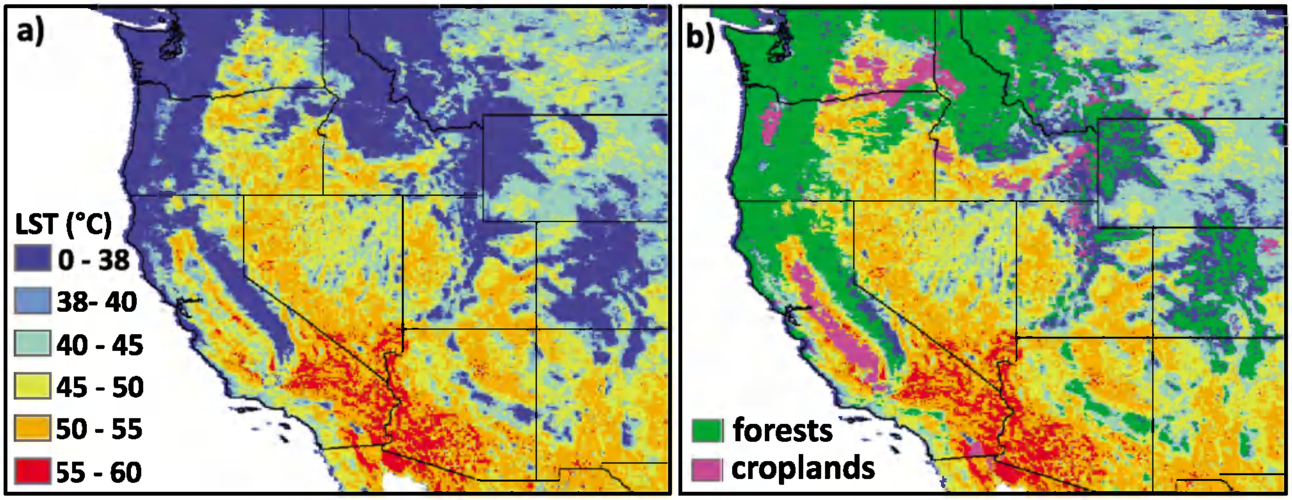

Figure 12. (a) The 2009 LST_{max} across the western United States displays complex patterns reflecting the seasonally arid and topographically complex region. (b) Forest cover shows close association with areas that do not exceed 38°C, and LST_{max} is artificially lowered over large areas due to cropland irrigation.

illustrates the value of the continuous spatial coverage of the satellite-derived LST_{max}.

[42] The western United States is characterized by a very strong hydrologic gradient that spans coastal temperate rain forests, and interior semiarid forests, and a pronounced summer dry period. Across the entire area there is strong spatial association between forest cover and complex patterns of LST_{max} that do not exceed 38°C (Figures 12a and 12b). In the interior West, mountains receive more precipitation than low-lying areas and are therefore wet enough to support forests. During the water-limited conditions when LST_{max} occurs, forests can access groundwater and sustain transpiration whereas other vegetation types cannot. This is a clear indication of the hydrologic cycle and the continuous interaction between a climate that is wet enough to support forests, and the transpiration from forests cooling LST_{max}.

[43] Closer examination does reveal that some of the driest ENF areas of the interior West do have LST_{max} values in the 40°C to 45°C range. These areas are also represented by a few ENF points above 40°C in Figure 9. Given that the data are analyzed at a 0.05° spatial resolution, the LST_{max} values in the forest-grassland ecotone could be significantly influenced by the large proportion of dry grasslands and bare soil within the sensor IFOV.

[44] Many cropland areas in the interior western United States are heavily irrigated in the summer due to the extremely arid conditions. The natural shrubland and grassland cover types are characterized by high LST_{max}, mostly between 50°C and 60°C. Irrigated croplands are easy to distinguish because they have LST_{max} values that are between 10°C and 15°C cooler than surrounding nonforested areas (Figures 12a and 12b). Croplands in California's Central Valley, the Snake River Plain, and the Columbia River Plateau, show close correspondence with areas where LST_{max} ranges from <38°C to 45°C.

[45] The LST_{max} during 2009 for the entire eastern United States is generally maintained below 38°C regardless of land cover type (image not presented). The driving factor for this pattern is the relatively wet and humid summer conditions that characterize the temperate deciduous forest biome, making water much less limiting when LST_{max} occurs compared to the western United States.

[46] In Europe a similar pattern exists between the semiarid forest ecosystems of the South and the temperate deciduous forests of the West and East (Figure 13). The Mediterranean climate of southern Europe is characterized by a pronounced summer dry period during which LST_{max} occurs. In southern Europe the location of forest cover shows a strong spatial association with areas where LST_{max} does not exceed 38°C (Figures 13a and 13b). The surrounding nonforest areas generally have much higher LST_{max}. West and East Europe are characterized by more moist, humid summer conditions, and both forest and nonforest areas are dominated by LST_{max} values that do not exceed 38°C (Figure 13b).

4. Summary and Conclusions

[47] We compared the LST_{max} from the Aqua/MODIS sensor to the corresponding site-based T_{amax} for every WMO station on Earth where T_{amax} is available. We first examined the relationship irrespective of land cover type, and as expected, a consistent positive correlation was observed between LST_{max} and T_{amax}. Our results show that as temperature increases and more thermal energy is concentrated at the Earth's surface, LST_{max} and T_{amax} become increasingly decoupled. At the highest temperatures, LST_{max} can be as much as 20°C higher than the corresponding T_{amax}. T_{air} can significantly underestimate the actual radiative surface temperature, especially at high temperatures and in nonforested areas. Because LST is more tightly coupled to the radiative and thermodynamic characteristics of the Earth's surface, it may be an improvement to substitute LST for T_{air} in calculations of the global average surface temperature in the radiative-convective equilibrium concept equation [*Pielke et al.*, 2007].

[48] We found the strength of the LST_{max}/T_{amax} relationship to be land-cover-dependent. At low temperatures, LST_{max} and T_{amax} are well coupled for all land cover types. Forests are the only cover type that maintains a strongly

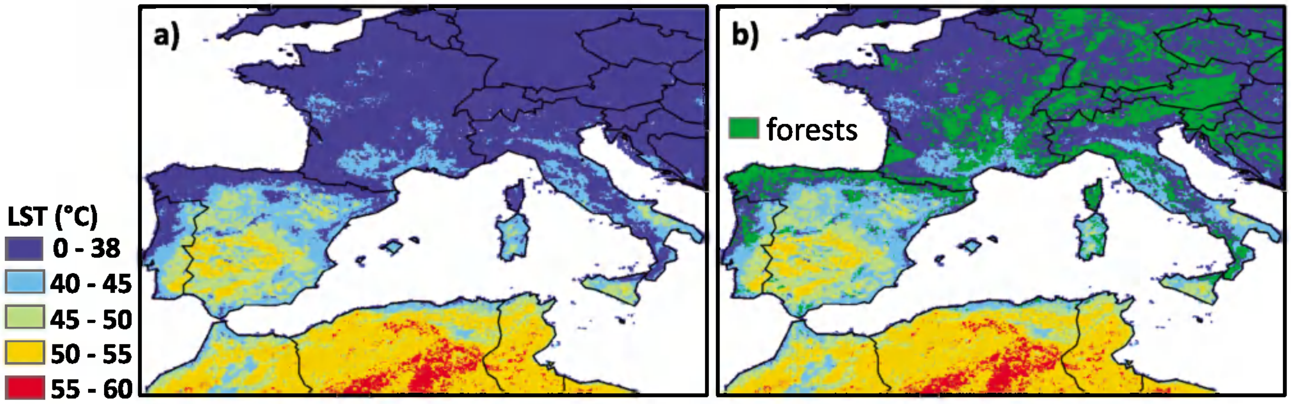

Figure 13. (a) The 2009 LST_{max} across Europe illustrates that in the arid Mediterranean climate of southern Europe, forests are closely coupled with areas where LST_{max} does not exceed 38°C. (b) In western and eastern Europe, moist, humid summers prevail, and the entire land area is generally maintained at or below 38°C.

coupled LST_{max}/T_{amax} relationship at highest temperatures and are distinct from the other land cover types because both LST_{max} and T_{amax} tend to range between the same values. The transpiration of forest ecosystems through the growing season dissipates more energy and lowers the Bowen ratio, and is the key driver for the stronger coupling of LST_{max} and T_{amax}. Forests cover over 21% of the Earth's surface and span a very large latitudinal gradient. The global regulation of surface temperature highlights the important role of forests in local, regional and global climate.

[49] Humans continue to dramatically influence global land cover through habitation, forest clearing, agriculture, and increasingly through anthropogenic driven climate change. This study reinforces the need to include land use and land cover change in holistic climate change studies and the important role that forests have in the global energy balance. Regarding policies proposed to influence forestry and land management practices for climate change-mitigation, the greatest uncertainties are in the biophysical influences that temperate forests have on climate [*Jackson et al.*, 2008]. This study shows that temperate forests characterized by a seasonal summer drought cycle, such as in western North America, have a similar cooling effect on LST_{max} and T_{amax} as tropical forests. A change to any other land cover type will result in a higher LST_{max}, with commensurate impacts on the surface energy balance and hydrologic cycle of the affected area. Temperate forests with moist, humid summers do not have the same cooling effect on the expression of LST_{max} and T_{amax} relative to the surrounding nonforested cover types because water is not limiting in the ecosystem during the time of thermal maxima.

[50] *LST* provides additional information on energy partitioning at the land surface-atmosphere boundary, and is more sensitive to changes in vegetation density compared to T_{air}. With continuous spatial coverage the satellite-derived LST_{max} data set may have value in studying the energy balance heterogeneity of the global land surface. The LST_{max} is a particularly robust metric of the canopy temperature because during high Sun around noon when maximum temperatures occur, more short-wave radiation penetrates deep into the canopy of vegetation [*Huband and Monteith*, 1986]. The multidimensional thermal view of the environment that accurate, satellite-derived LST provides is critical to the actual experience of many organisms.

[51] The unique information provided by *LST* compared to T_{air} also enhances the benefits of combining these two variables together. Our findings suggest that the LST_{max}/T_{amax} relationship presents new ways to track climate change, especially as these changes impact one climatological variable more than the other. For example, should summers become warmer in the cryosphere, as predicted by climate change, more snow free areas and drier soil conditions would result in the LST_{max} rising faster than the T_{amax}. These long-term trends in the LST_{max}/T_{amax} relationship would need to be tracked for decades. It may be important to further compare these data sets with other satellite based and ground based data sets such as the MODIS Albedo product, and with data from Fluxnet sites.

[52] **Acknowledgments.** This effort was sponsored by the MODIS Project (NNX08AG87A). We thank the reviewers and Lucas Jones for valuable comments.

References

Albright, T. P., A. M. Pidgeon, C. D. Rittenhouse, M. K. Clayton, C. H. Flather, P. D. Culbert, and V. C. Radeloff (2011), Heat waves measured with MODIS land surface temperature data predict changes in avian community structure, *Remote Sens. Environ.*, *115*, 245–254, doi:10.1016/j.rse.2010.08.024.

Anderson, M. C., J. M. Norman, J. R. Mecikalski, J. A. Otkin, and W. P. Kustas (2007), A climatological study of evapotranspiration and moisture stress across the continental United States based on thermal remote sensing: 2. Surface moisture climatology, *J. Geophys. Res.*, *112*, D11112, doi:10.1029/2006JD007507.

Anderson, R. G., et al. (2011), Biophysical considerations in forestry for climate protection, *Front. Ecol. Environ*, *9*, 174–182, doi:10.1890/090179.

Bala, G., K. Caldeira, M. Wickett, T. J. Phillips, D. B. Lobell, C. Delire, and A. Mirin (2007), Combined climate and carbon-cycle effects of large-scale deforestation, *Proc. Natl. Acad. Sci. U.S.A.*, *104*, 6550–6555.

Baldocchi, D. D., L. Xu, and N. Kiang (2004), How plant functional-type, weather, seasonal drought, and soil physical properties alter water and energy fluxes of an oak-grass savanna and an annual grassland, *Agric. For. Meteorol.*, *123*, 13–39, doi:10.1016/j.agrformet.2003.11.006.

Becker, F., and Z.-L. Li (1990), Toward a local split-window method over land surface, *Int. J. Remote Sens.*, *11*(3), 369–393, doi:10.1080/01431169008955028.

Betts, R. A. (2000), Offset of the potential carbon sink from boreal forestation by decreases in surface albedo, *Nature*, *408*, 187–190, doi:10.1038/35041545.

Bonan, G. B. (2008), Forests and climate change: Forcings, feedbacks, and the climate benefits of forests, *Science*, *320*, 1444–1449, doi:10.1126/science.1155121.

Chapin, F. S., III, J. T. Randerson, A. D. McGuire, J. A. Foley, and C. B. Field (2008), Changing feedbacks in the climate-biosphere system, *Front. Ecol. Environ*, *6*, 313–320, doi:10.1890/080005.

Choudhury, B. J. (1989), Estimating evaporation and carbon assimilation using infrared temperature data: Vistas in modeling, in *Theory and Applications of Remote Sensing*, edited by G. Asrar, pp. 628–690, Wiley, New York.

Coops, N. C., M. A. Wulder, and D. Iwanicka (2009), Large area monitoring with a MODIS-based Disturbance Index (DI) sensitive to annual seasonal variations, *Remote Sens. Environ.*, *113*, 1250–1261, doi:10.1016/j.rse.2009.02.015.

Davey, C. A., R. A. Pielke Sr., and K. P. Gallo (2006), Differences between near-surface equivalent temperature and temperature trends for the eastern United States: Equivalent temperature as an alternative measure of heat content, *Global Planet. Change*, *54*, 19–32, doi:10.1016/j.gloplacha.2005.11.002.

Friedl, M. A., and F. W. Davis (1994), Sources of variation in radiometric surface temperature over a tallgrass prairie, *Remote Sens. Environ.*, *48*, 1–17, doi:10.1016/0034-4257(94)90109-0.

Friedl, M. A., et al. (2002), Global land cover from MODIS: Algorithms and early results, *Remote Sens. Environ.*, *83*, 287–302, doi:10.1016/S0034-4257(02)00078-0.

Garratt, J. R. (1992), Extreme maximum land surface temperatures, *J Appl. Meteorol.*, *31*, 1096–1105, doi:10.1175/1520-0450(1992)031<1096:EMLST>2.0.CO;2.

Gates, D. M. (1965), Energy, plants, and ecology, *Ecology*, *46*, 1–13, doi:10.2307/1935252.

Gay, L. W. (1972), Radiative temperatures in the Willamette Valley, *Northwest Sci.*, *46*, 332–335.

Goward, S. N., G. D. Cruickshanks, and A. S. Hope (1985), Observed relation between thermal emission and reflected spectral radiance of a complex vegetated landscape, *Remote Sens. Environ.*, *18*, 137–146, doi:10.1016/0034-4257(85)90044-6.

Hale, R. C., K. P. Gallo, T. W. Owen, and T. R. Loveland (2006), Land use/land cover change effects on temperature trends at U.S. Climate Normals stations, *Geophys. Res. Lett.*, *33*, L11703, doi:10.1029/2006GL026358.

Hansen, J., M. Sato, R. Ruedy, K. Lo, D. W. Lea, and M. Medina-Elizade (2006), Global temperature change, *Proc. Natl. Acad. Sci. U. S. A.*, *103*, 14,288–14,293, doi:10.1073/pnas.0606291103.

Hansen, M. C., et al. (2008), Humid tropical forest clearing from 2000 to 2005 quantified by using multitemporal and multiresolution remotely sensed data, *Proc. Natl. Acad. Sci. U. S. A.*, *105*, 9439–9444, doi:10.1073/pnas.0804042105.

Hoffmann, W. A., and R. B. Jackson (2000), Vegetation-climate feedbacks in the conversion of tropical savanna to grassland, *J. Clim.*, *13*, 1593–1602, doi:10.1175/1520-0442(2000)013<1593:VCFITC>2.0.CO;2.

Huband, N. D. S., and J. L. Monteith (1986), Radiative surface temperature and energy balance of a wheat canopy, *Boundary Layer Meteorol.*, *36*, 1–17, doi:10.1007/BF00117455.

Hutyra, L. R., J. W. Munger, S. R. Saleska, E. Gottlieb, B. C. Daube, A. L. Dunn, D. F. Amaral, P. B. de Camargo, and S. C. Wofsy (2007), Seasonal controls on the exchange of carbon and water in an Amazonian rain forest, *J. Geophys. Res.*, *112*, G03008, doi:10.1029/2006JG000365.

Intergovernmental Panel on Climate Change (2007), Climate change 2007: The physical science basis, in *Contribution of Working Group I to the Fourth Assessment. Report of the Intergovernmental Panel on Climate Change*, edited by S. Solomon et al., Cambridge Univ. Press, Cambridge, U. K.

Jackson, R. B., et al. (2008), Protecting climate with forests, *Environ. Res. Lett.*, *3*, 044006, doi:10.1088/1748-9326/3/4/044006.

Jacob, F., F. Petitcolin, T. Schmugge, E. Vermote, A. French, and K. Ogawa (2004), Comparison of land surface emissivity and radiometric temperature derived from MODIS and ASTER sensors, *Remote Sens. Environ.*, *90*, 137–152, doi:10.1016/j.rse.2003.11.015.

Jin, M., and R. E. Dickinson (2010), Land surface skin temperature climatology: Benefitting from the strengths of satellite observations, *Environ. Res. Lett.*, *5*, 044004, doi:10.1088/1748-9326/5/4/044004.

Julien, Y., and J. A. Sobrino (2009), The Yearly Land Cover Dynamics (YLCD) method: An analysis of global vegetation from NDVI and LST parameters, *Remote Sens. Environ.*, *113*, 329–334, doi:10.1016/j.rse.2008.09.016.

Kalnay, E., M. Cai, H. Li, and J. Tobin (2006), Estimation of the impact of land-surface forcings on temperature trends in eastern Unites States, *J Geophys. Res.*, *111*, D06106, doi:10.1029/2005JD006555.

Karl, T. R., C. D. Miller, and W. L. Murray (2006), *Temperature Trends in the Lower Atmosphere: Steps for Understanding and Reconciling* Differences, edited by T. R. Karl et al., U.S. Clim. Change Sci. Program and the Subcomm. on Global Change Res., Washington, D. C.

King, M. D. (1999), *EOS Science Plan: The State of Science in the EOS Program*, 397 pp., NASA, Washington, D. C.

Knapp, A. K., and M. D. Smith (2001), Variation among biomes in temporal dynamics of aboveground primary production, *Science*, *291*, 481–484, doi:10.1126/science.291.5503.481.

Lambin, E. F., and D. Ehrlich (1996), The surface temperature-vegetation index space for land cover and land-cover change analysis, *Int. J Remote Sens.*, *17*, 463–487, doi:10.1080/01431169608949021.

Linacre, E. T. (1964), A note on a feature of leaf and air temperatures, *Agric. Meteorol.*, *1*, 66–72, doi:10.1016/0002-1571(64)90009-3.

Loarie, S. R., D. B. Lobell, G. P. Asner, Q. Mu, and C. B. Field (2011), Direct impacts on local climate of sugar-cane expansion in Brazil, *Nat. Clim. Change*, *1*, 105–109, doi:10.1038/nclimate1067.

Loveland, T. R., and A. S. Belward (1997), The IGBP-DIS global 1-km land cover data set, DIScover: First results, *Int. J. Remote Sens.*, *65*, 1021–1031.

Mannstein, H. (1987), Surface energy budget, surface temperature and thermal inertia, in *Remote Sensing Applications in Meteorology and Climatology*, edited by R. A. Vaughan, pp. 391–410, D. Reidel, Dordrecht, Netherlands.

Marland, G., et al. (2003), The climatic impacts of land surface change and carbon management, and the implications for climate-change mitigation policy, *Clim. Policy*, *3*, 149–157.

Mildrexler, D. J., M. Zhao, and S. W. Running (2006), Where are the hottest spots on Earth?, *EOS Trans. AGU*, *87*(43), 461, 467, doi:10.1029/2006EO430002.

Mildrexler, D. J., M. Zhao, F. A. Heinsch, and S. W. Running (2007), A new satellite-based methodology for continental scale disturbance detection, *Ecol. Appl.*, *17*, 235–250, doi:10.1890/1051-0761(2007)017[0235:ANSMFC]2.0.CO;2.

Mildrexler, D. J., M. Zhao, and S. W. Running (2009), Testing a MODIS global disturbance index across North America, *Remote Sens. Environ.*, *113*, 2103–2117, doi:10.1016/j.rse.2009.05.016.

Mildrexler, D. J., M. Zhao, and S. W. Running (2011), Satellite finds highest land skin temperatures on Earth, *Bull. Am. Meteorol. Soc.*, *92*, 855–860, doi:10.1175/2011BAMS3067.1.

Monteith, J. L. (1981), Evaporation and surface temperature, *Q. J. R. Meteorol. Soc.*, *107*, 1–27, doi:10.1256/smsqj.45101.

Montenegro, A., M. Eby, Q. Mu, M. Mulligan, A. J. Weaver, E. C. Wiebe, and M. Zhao (2009), The net carbon drawdown of small scale afforestation from satellite observations, *Global Planet. Change*, *69*, 195–204, doi:10.1016/j.gloplacha.2009.08.005.

Morton, D. C., R. S. DeFries, Y. E. Shimabukuro, L. O. Anderson, E. Arai, F. del Bon Espirito-Santo, R. Freitas, and J. Morisette (2006), Cropland expansion changes deforestation dynamics in the southern Brazilian Amazon, *Proc. Natl. Acad. Sci. U. S. A.*, *103*, 14,637–14,641, doi:10.1073/pnas.0606377103.

Mu, Q., F. A. Heinsch, M. Zhao, and S. W. Running (2007), Development of a global evapotranspiration algorithm based on MODIS and global meteorology data, *Remote Sens. Environ.*, *111*, 519–536, doi:10.1016/j.rse.2007.04.015.

Nemani, R. R., and S. W. Running (1989), Estimation of regional surface resistance to evapotranspiration from NDVI and thermal-IR AVHRR data, *J. Appl. Meteorol.*, *28*, 276–284, doi:10.1175/1520-0450(1989)028<0276:EORSRT>2.0.CO;2.

Nemani, R. R., and S. W. Running (1997), Land cover characterization using multitemporal red, near-IR, and thermal-IR data from NOAA/AVHRR, *Ecol. Appl.*, *7*, 79–90, doi:10.1890/1051-0761(1997)007[0079:LCCUMR]2.0.CO;2.

Nemani, R. R., L. L. Pierce, and S. W. Running (1993), Developing satellite derived estimates of surface moisture status, *J. Appl. Meteorol.*, *32*, 548–557, doi:10.1175/1520-0450(1993)032<0548:DSDEOS>2.0.CO;2.

Nemani, R. R., S. W. Running, R. A. Pielke, and T. N. Chase (1996), Global vegetation changes from coarse resolution satellite data, *J Geophys. Res.*, *101*, 7157–7162, doi:10.1029/95JD02138.

Norman, J. M., and F. Becker (1995), Terminology in thermal infrared remote sensing of nature surfaces, *Agric. For. Meteorol.*, *77*, 153–166, doi:10.1016/0168-1923(95)02259-Z.

Peel, R. F. (1974), Insolation weathering: Some measurements of diurnal temperature changes in exposed rocks in the Tibetsi region, central Sahara, *Z. Geomorph. N. F.*, *21*, 19–28.

Pielke, R. A., Sr., et al. (2007), Unresolved issues with the assessment of multidecadal global land surface temperature trends, *J. Geophys. Res.*, *112*, D24S08, doi:10.1029/2006JD008229.

Price, J. C. (1984), Land surface temperature measurements from the split window channels of the NOAA 7 advanced very high resolution radiometer, *J. Geophys. Res.*, *89*, 7231–7237, doi:10.1029/JD089iD05p07231.

Priestley, C. H. B. (1966), The limitation of temperature by evaporation in hot climates, *Agric. Meteorol.*, *3*(314), 241–246.

Priestley, C. H. B., and R. J. Taylor (1972), On the assessment of surface heat flux and evaporation using large-scale parameters, *Mon. Weather Rev.*, *100*, 81–92, doi:10.1175/1520-0493(1972)100<0081:OTAOSH>2.3.CO;2.

Qin, Z., G. D. Olmo, and A. Karnieli (2001), Derivation of split window algorithm and its sensitivity analysis for retrieving land surface temperature from NOAA-advanced very high resolution radiometer data, *J Geophys. Res.*, *106*, 22,655–22,670, doi:10.1029/2000JD900452.

Running, S. W. (2008), Ecosystem disturbance, carbon, and climate, *Science*, *321*, 652–653, doi:10.1126/science.1159607.

Running, S. W., R. R. Nemani, F. A. Heinsch, M. Zhao, M. Reeves, and H. Hashimoto (2004), A continuous satellite-derived measure of global terrestrial primary production, *BioScience*, *54*, 547–560, doi:10.1641/0006-3568(2004)054[0547:ACSMOG]2.0.CO;2.

Schmugge, T. J., and F. Becker (1991), Remote sensing observations for the monitoring of land-surface fluxes and water budgets, in *Land Surface Evaporation: Measurements and Parameterization*, edited by T. J. Schmugge and J. C. Andre, Springer, New York.

Sellers, P. J., F. G. Hall, G. Asrar, D. E. Strebel, and R. E. Murphy (1988), The first ISLSCP Field Experiment (FIFE), *Bull. Am. Meteorol. Soc.*, *69*, 22–27, doi:10.1175/1520-0477(1988)069<0022:TFIFE>2.0.CO;2.

Sinclair, J. G. (1922), Temperatures of the soil and air in a desert, *Mon. Weather Rev.*, *50*, 142–144, doi:10.1175/1520-0493(1922)50<142b:TOTSAA>2.0.CO;2.

Snyder, W. C., Z. Wan, Y. Zhang, and Y.-Z. Feng (1998), Classification-based emissivity for land surface temperature measurement from space, *Int. J Remote Sens.*, *19*, 2753–2774, doi:10.1080/014311698214497.

Wan, Z., and J. Dozier (1989), Land-surface temperature measurement from space: Physical principles and inverse modeling, *IEEE Trans. Geosci. Remote Sens.*, *27*, 268–278, doi:10.1109/36.17668.

Wan, Z., and J. Dozier (1996), A generalized split-window algorithm for retrieving land-surface temperature from space, *IEEE Trans. Geosci. Remote Sens.*, *34*, 892–905, doi:10.1109/36.508406.

Wan, Z., and Z. L. Li (1997), A physics-based algorithm for retrieving land-surface emissivity and temperature from EOS/MODIS data, *IEEE Trans. Geosci. Remote Sens.*, *35*, 980–996, doi:10.1109/36.602541.

Wan, Z., and Z. L. Li (2011), MODIS land surface temperature and emissivity, in *Land Remote Sensing and Global Environmental Change, Remote Sens. and Digital Image Proc.*, vol. 11, edited by B. Ramachandran et al., pp. 563–577, Springer, New York.

Wan, Z. M., Y. L. Zhang, Q. C. Zhang, and Z. L. Li (2003), Validation of the land-surface temperature products retrieved from Terra Moderate Resolution Imaging Spectroradiometer data, *Remote Sens. Environ.*, *83*, 163–180.

Wan, Z., Y. Zhang, Q. Zhang, and Z.-L. Li (2004a), Quality assessment and validation of the MODIS global land surface temperature, *Int. J. Remote Sens.*, *25*, 261–274, doi:10.1080/0143116031000116417.

Wan, Z., P. Wang, and Z. Li (2004b), Using MODIS Surface Temperature and Normalized Difference Vegetation Index products for monitoring drought in the southern Great Plains, USA, *Int. J. Remote Sens.*, *25*, 61–72.

Waring, R. H. (2002), Temperate coniferous forests, in *Encyclopedia of Global Environmental Change*, vol. 2, John Wiley, Chichester, U. K.

White, A. B., P. Kumar, and D. Tcheng (2005), A data mining approach for understanding topographic control on climate-induced inter-annual vegetation variability over the United States, *Remote Sens. Environ.*, *98*, 1–20, doi:10.1016/j.rse.2005.05.017.

Zhao, M., F. A. Heinsch, R. R. Nemani, and S. W. Running (2005), Improvements of the MODIS terrestrial gross and net primary production global data set, *Remote Sens. Environ.*, *95*, 164–176, doi:10.1016/j.rse.2004.12.011.

D. J. Mildrexler, S. W. Running, and M. Zhao, Numerical Terradynamic Simulation Group, Department of Ecosystem and Conservation Sciences, University of Montana, Missoula, MT 59812, USA. (drexler@ntsg.umt.edu)